ENSO's Modulation of Water Vapor Transport over the Pacific–North American Region

HYE-MI KIM

School of Marine and Atmospheric Sciences, Stony Brook University, Stony Brook, New York

MICHAEL A. ALEXANDER

NOAA/Earth System Research Laboratory, Boulder, Colorado

(Manuscript received 23 October 2014, in final form 6 February 2015)

ABSTRACT

The vertically integrated water vapor transport (IVT) over the Pacific–North American sector during three phases of ENSO in boreal winter (December–February) is investigated using IVT values calculated from the Climate Forecast System Reanalysis (CFSR) during 1979–2010. The shift of the location and sign of sea surface temperature (SST) anomalies in the tropical Pacific Ocean leads to different atmospheric responses and thereby changes the seasonal mean moisture transport into North America. During eastern Pacific El Niño (EPEN) events, large positive IVT anomalies extend northeastward from the subtropical Pacific into the northwestern United States following the anomalous cyclonic flow around a deeper Aleutian low, while a southward shift of the cyclonic circulation during central Pacific El Niño (CPEN) events induces the transport of moisture into the southwestern United States. In addition, moisture from the eastern tropical Pacific is transported from the deep tropical eastern Pacific into Mexico and the southwestern United States during CPEN. During La Niña (NINA), the seasonal mean IVT anomaly is opposite to that of two El Niño phases. Analyses of 6-hourly IVT anomalies indicate that there is strong moisture transport from the North Pacific into the northwestern and southwestern United States during EPEN and CPEN, respectively. The IVT is maximized on the southeastern side of a low located over the eastern North Pacific, where the low is weaker but located farther south and closer to shore during CPEN than during EPEN. Moisture enters the southwestern United States from the eastern tropical Pacific during NINA via anticyclonic circulation associated with a ridge over the southern United States.

1. Introduction

Heavy winter precipitation in the western United States is significantly affected by long narrow bands of water vapor transport from the tropical/subtropical North Pacific into midlatitudes. Often these water vapor plumes originate near Hawaii and are known colloquially as the "Pineapple Express" (e.g., Lackmann and Gyakum 1999). The more general case of strong tropical–extratropical water vapor transport was termed "tropospheric rivers" by Newell et al. (1992) and then "atmospheric rivers" (ARs) by Zhu and Newell (1998). ARs generally occur ahead of cold fronts associated with winter storms. The maximum number of ARs occurs over the northeastern Pacific Ocean and after landfall they induce nearly twice as much precipitation as non-AR storms in the western United States (Zhu and Newell 1998; Neiman et al. 2008; Waliser et al. 2012). The critical role of ARs in hydrometeorological extremes, such as the total amount of precipitation, streamflow, and mountain snowpack in the western United States, has been extensively explored while the AR–precipitation relationship heavily depends on the definition of an AR (Dettinger 2004; Ralph et al. 2006; Dettinger et al. 2011; Neiman et al. 2011; Warner et al. 2012; Guan et al. 2012, 2013).

While ARs provide a useful framework for storm-based moisture transport, the definition of an AR is subjective; that is, it is based on an arbitrary length, width, and magnitude of a plume of the vertically integrated water vapor (IWV) or integrated water vapor transport (IVT). Therefore, depending on the definition, one can

Corresponding author address: Hye-Mi Kim, School of Marine and Atmospheric Sciences, Stony Brook University, Stony Brook, NY 11794.
E-mail: hyemi.kim@stonybrook.edu

DOI: 10.1175/JCLI-D-14-00725.1

get very different measures of ARs and their overall impact on precipitation. For example, Rutz et al. (2014) compared ARs defined using both IVT and IWV and found sizable differences in frequency and duration of events, especially in the inland penetration of moisture. In addition, non-AR processes, such as cutoff lows or cases where the moisture comes from the extratropics as opposed to the subtropics, can also lead to precipitation in the western North America. Therefore, in this study, we do not identify ARs, but rather examine the IVT and its impact on precipitation directly.

While the variability of water vapor transport and ARs have been studied extensively on synoptic time scales, only a few recent studies have explored the link between the water vapor transport and large-scale climate variability on subseasonal-to-interannual time scales. Jiang and Deng (2011) and Jiang et al. (2014) linked East Asian cold surges with subsequent AR activity over the eastern North Pacific and western North America. Guan et al. (2012) found a strong connection between AR landfalls in the Sierra Nevada and the Madden–Julian oscillation (MJO; Madden and Julian 1972), especially when the MJO-driven convection is located over the tropical western Pacific. Guan et al. (2013) examined the influence of the Arctic Oscillation (AO) and Pacific–North American (PNA) mode on water vapor transport and the Sierra Nevada snowpack. The coexistence of the negative phases of AO and PNA induces favorable condition for southwesterly winds impinging on the Sierra Nevada, enhancing the water vapor transport, snowfall, and the mountain snowpack (Guan et al. 2013).

El Niño–Southern Oscillation (ENSO), which results from large-scale ocean–atmosphere interaction in the tropical Pacific, influences the global climate via changes in the atmospheric circulation, especially over the PNA region (e.g., Ropelewski and Halpert 1987). The precipitation amount over the North Pacific and United States varies between the warm (El Niño) and cold (La Niña) phases of ENSO, while the teleconnection between ENSO and U.S. precipitation varies with time (van Oldenborgh and Burgers 2005; Mo 2010). Given that ENSO modulates both the large-scale circulation and the precipitation amount, it is natural to ask how the moisture transport from tropical and extratropical Pacific to North America would be affected by ENSO variability. The connection between ENSO and moisture transport, however, has received limited attention. Dettinger (2004) and Bao et al. (2006) hypothesized that the neutral ENSO phase is the most favorable condition for the direct entrainment of tropical water vapor into the west coast of North America, while the warm phase of ENSO results in an unfavorable condition for water vapor transport by strengthening the subtropical ridge. In contrast, the results of Guan et al. (2013) suggest that the warm phase of ENSO is more favorable for stronger ARs than the cold phase of ENSO. However, while Guan et al. (2013) examined the influence of ENSO on ARs, they focused on the impact on California rather than the whole North American coast and limited their analysis to a brief recent period (1998–2011). Moreover, the different types of ENSO may impact where the ARs and associated moisture transport reach North America and penetrate into the interior. Therefore, we investigate the impact of different types of ENSO events on moisture transport over the North Pacific and western North America during a 32-yr period.

Recent studies have suggested that the warm phase of ENSO can be distinguished into two distinct types based on the spatial distribution of SST anomalies in the tropical Pacific Ocean (Ashok et al. 2007; Kao and Yu 2009; Kug et al. 2009, and many others). In eastern Pacific (EP) El Niño years, or canonical El Niño events, the SST anomaly is maximized near the coast of South America to about 150°W, whereas in central Pacific (CP) El Niño years the SST anomaly maximum is located farther west, near the date line. This CP-type El Niño has occurred more frequently in the recent decade (Kug et al. 2009; Yeh et al. 2009; Lee and McPhaden 2010). While it is still controversial as to whether there are two distinct forms of El Niño or a continuum of warm ENSO states (Newman et al. 2011a,b; Johnson 2013; Capotondi et al. 2015), the shift in the location of SST anomalies leads to different atmospheric responses, which have significantly different impacts on North American climate (Barsugli and Sardeshmukh 2002; Mo 2010; Yu et al. 2012; Yu and Zou 2013). While EP El Niño forcing excites a wave train emanating from the tropical Pacific into the southern United States, which projects strongly on the tropical Northern Hemisphere pattern, CP El Niño excites a wave train resembling the PNA pattern (Mo 2010; Yu et al. 2012). In conjunction with these large scale-circulation changes, the jet steam and storm track shift south in CP relative to EP Niño events, thereby increasing the precipitation in the southwestern United States (Mo 2010; Yu and Zou 2013).

In this study, we will examine how the three ENSO categories, EP El Niño (EPEN), CP El Niño (CPEN), and La Niña (NINA) modulate the large-scale atmospheric circulation variability, and thereby change the water vapor transport into western North America. Improved understanding of the influence of ENSO on the water vapor transport may enhance seasonal prediction of heavy precipitation and floods in the western United States. The paper is organized as follows: the data are described in section 2; the seasonal and variations at 6-h

and longer time scales of water vapor transport and their associated circulation fields during the three ENSO phases are examined in sections 3 and 4, respectively. The results are summarized in section 5.

2. Data

IVT is defined as

$$\mathrm{IVT} = \frac{1}{g}\int_{\mathrm{Psfc}}^{300\mathrm{hPa}} q\mathbf{V}\,dp,$$

where g is the gravitational acceleration, $\mathbf{V}$ is the vector wind, p is the pressure, and q is the specific humidity. The water vapor transport is vertically integrated from the surface to 300 hPa with 6-hourly data over a portion of the Northern Hemisphere (10°–75°N, 160°E–60°W). The specific humidity, wind, and geopotential height fields are obtained from National Oceanic and Atmospheric Administration (NOAA) Climate Forecast System Reanalysis (CFSR; Saha et al. 2010). The CFSR is the product of a coupled ocean–atmosphere–land system, where the resolution of the spectral atmospheric model is T382 (~40 km) with 64 vertical levels. The resolution of CFSR is finer than NCEP reanalysis versions 1 and 2 used in many previous AR studies. The analysis fields are archived on a 0.5° latitude and longitude grid at 6-h intervals from January 1979 to December 2010. SST data are obtained from monthly NOAA Optimum Interpolation SST version 2 (Reynolds et al. 2002) and the precipitation from the Global Precipitation Climatology Project (GPCP) version 2.2 (Adler et al. 2003).

We focus on the boreal winter season from December to February (DJF). ENSO phases are classified in three categories. EP El Niño winters (four seasons: 1982/83, 1986/87, 1997/98, and 2006/07, hereafter EPEN) and CP El Niño winters (four seasons: 1994/95, 2002/03, 2004/05, and 2009/10, hereafter CPEN) are selected based on the classification in Yu and Zou (2013), who identified the EP and CP El Niño years by the majority consensus from various EP/CP index classification methods. Unlike El Niño events, La Niña events are less distinctive in terms of spatial structure (Kug et al. 2009; Kug and Ham 2011) and thus are not separated into different phases. Therefore, La Niña winters are selected based on the Niño-3.4 index (four seasons: 1988/89, 1998/99, 1999/2000, and 2007/08, hereafter NINA). The 19 years that are not in the EPEN, CPEN, or NINA categories are selected as neutral years. A bootstrap technique is applied to determine statistical significance of the composite anomalies. For each ENSO event, a composite anomaly is constructed with 4 years chosen at random from among the 31 years of data and then this process is repeated 10 000 times to obtain a probability distribution at the 90% level.

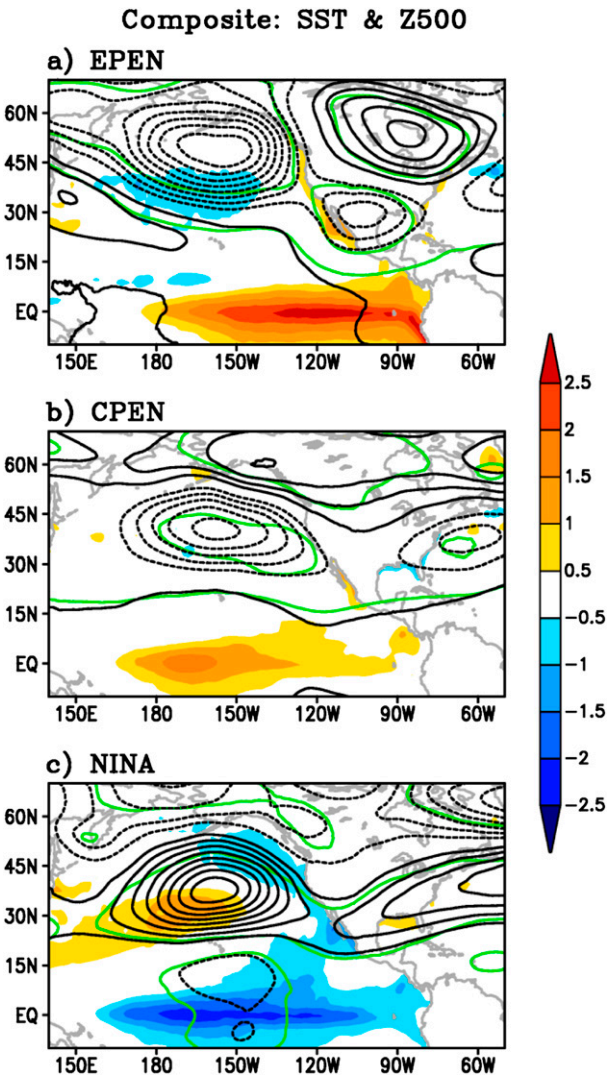

FIG. 1. Composite of seasonal mean (DJF) SST anomaly (K; shading) and 500-hPa geopotential height (Z500) anomaly (m; contour) for (a) EPEN, (b) CPEN, and (c) NINA. The Z500 contour interval is 10 m. Solid contours are positive, dashed contours are negative, and the zero contours are omitted. Green contours show statistical significance at the 90% level for Z500 obtained by a bootstrap method.

3. Modulation of seasonal water vapor transport by ENSO

Composite maps of the boreal winter SST anomaly and 500-hPa geopotential height (Z500) anomalies during the three ENSO categories are shown in Fig. 1. Contours indicate statistical significance of the Z500 anomalies at the 90% level. The maximum SST anomaly

in CPEN (Fig. 1b) is reduced in magnitude and shifted westward toward the central equatorial Pacific Ocean relative to EPEN events (Fig. 1a), similar to results in previous studies (Kug et al. 2009; Yeh et al. 2009; Lee and McPhaden 2010; Yu et al. 2012; Yu and Zou 2013). NINA years show a broad negative SST anomaly extending from 150°E to the South American coast. The corresponding large-scale atmospheric circulation anomalies in three ENSO categories exhibit distinct characteristics. In both El Niño phases, a low pressure anomaly occurs over the North Pacific Ocean associated with an eastward shift and an intensification of the Aleutian low. This deep trough is centered near 50°N, 150°W for EPEN, whereas the low is shifted to the southwest, centered near 37°N, 160°W, and is reduced in amplitude for CPEN. The opposite to both El Niño phases, with an anomalous high over the eastern North Pacific, occurs during La Niña events (Fig. 1; also see Yeh et al. 2009; Yu et al. 2012). While the atmospheric response pattern to NINA forcing is the opposite to both types of El Niño events, the pattern more closely resembles the inverse of CPEN than EPEN. As described earlier, La Niña events are less variable in longitude, since the SST anomalies during cold events are already shifted to the west relative to conventional El Niño events (Kug et al. 2009; Kug and Ham 2011).

Composite maps of the magnitude and direction of the anomalous IVT during winter for the three categories of ENSO are shown in Fig. 2. EPEN events exhibit large positive IVT anomalies extending northeastward from the subtropical Pacific into the northwestern United States along the anomalous cyclonic flow (Fig. 2a). Significant negative IVT anomalies are found over the subtropical North Pacific (20°–30°N), likely due to northerly flow, and over the United States where easterlies from the relatively dry continent restrict the transport of moisture.

Associated with the equatorward shift of the cyclonic circulation over the North Pacific in CPEN relative to EPEN, the anomalous IVT also shifts south (Fig. 2b). The southeastern edge of the cyclonic circulation extends toward North America at about 30°N and transports moisture into the far southwestern United States. Given that the moisture is generally higher at lower latitudes, the southward shift of the cyclonic circulation in CPEN may transport more water vapor into the United States even though the circulation intensity is weaker than during EPEN. There is also a direct path from the deep tropics into Mexico and extending into the southwestern United States in CPEN that is distinct from the large-scale cyclonic circulation over the North Pacific (Fig. 2b).

In NINA, the seasonal mean IVT anomaly is opposite to the anomalies during the two El Niño phases. A significant positive IVT anomaly occurs between 35° and 50°N west of 140°W, associated with the anticyclonic circulation response to La Niña SST anomalies (Fig. 2c). Significant negative IVT anomalies around 30°N occur on the southern side of the anticyclonic anomaly, likely associated with the advection of relatively cold and dry air. In the subtropics (10°–20°N), flow off Mexico results in reduced IVT over the far eastern Pacific, while farther offshore the circulation anomalies result in stronger trade winds (e.g., see Larkin and Harrison 2002), which could enhance evaporation and lead to positive IVT

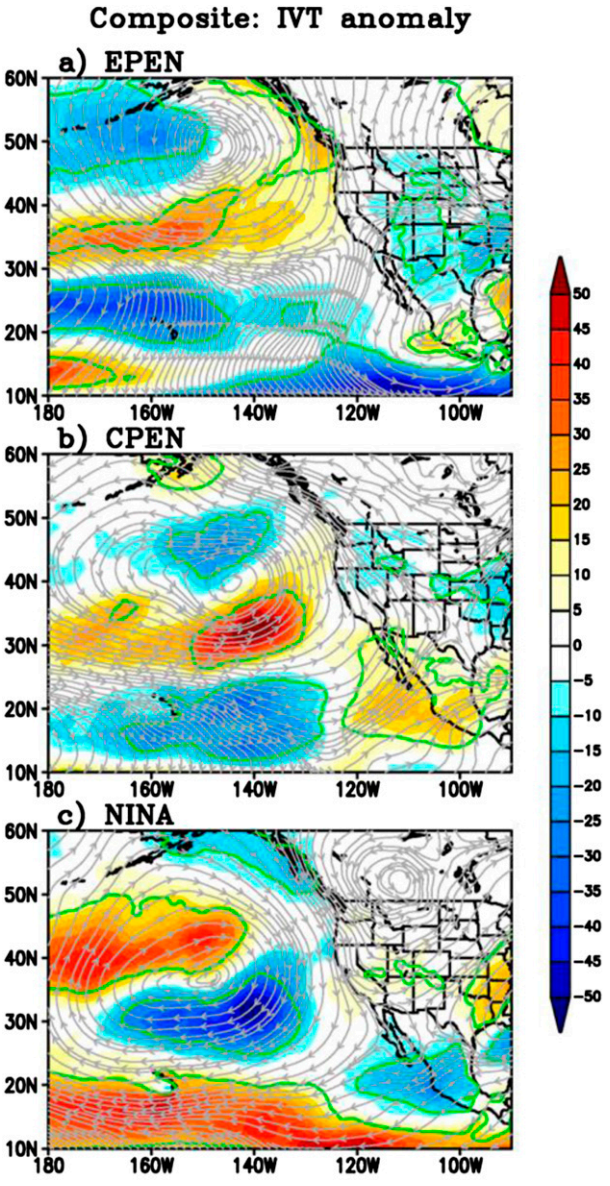

FIG. 2. Composite of seasonal mean (DJF) IVT magnitude anomaly (kg m^{-1} s^{-1}; shading) and the streamlines of direction of the mean IVT anomaly for (a) EPEN, (b) CPEN, and (c) NINA. Green contours show statistical significance at the 90% level for IVT magnitude.

anomalies. Weak positive IVT anomalies occur over most of the western United States associated with northerly flow.

The land-only precipitation anomalies during the three ENSO categories are shown in Fig. 3. The northwestern United States and southwestern Canada (region A: 40°–58°N, 130°–120°W; precipitation averaged only over land within the purple box in Fig. 3) experience enhanced precipitation relative to climatology in EPEN, but reduced precipitation in CPEN (Fig. 3b), which is consistent with the results from Yu and Zou (2013). However, the enhanced precipitation in region A for EPEN mainly results from two super El Niños (1982/83 and 1997/98), while the moderate El Niño cases (1986/87 and 2009/10) are near normal (Yu and Zou 2013), as discussed further in section 5. During NINA events, the precipitation in region A is slightly above normal (Fig. 3c). The precipitation anomaly is 0.81 mm day^{-1} for EPEN, −0.56 mm day^{-1} for CPEN, and 0.24 mm day^{-1} for NINA in region A (Fig. 4). The positive precipitation anomaly averaged over the southwestern United States (region B: 20°–40°N, 122°–108°W; black box in Fig. 3) is the greatest for CPEN among the ENSO categories with values of 0.18 mm day^{-1} for EPEN, 0.47 mm day^{-1} for CPEN, and −0.31 mm day^{-1} for NINA (Fig. 4). For CPEN, the precipitation anomaly is positive over California, Arizona, and Mexico, where the IVT anomaly is also positive. In EPEN, the precipitation anomaly is slightly positive in region B despite a negative IVT anomaly. However, while IVT is critical for bringing moisture to the western United States in winter, precipitation is directly related to moisture flux convergence ($\mathbf{V} \cdot \mathrm{IVT}$).

4. Modulation of 6-h IVT and height variability by ENSO

Next, we investigate the characteristics of IVT variability based on anomalies obtained by subtracting the long-term (1979–2010) monthly mean from the instantaneous 6-h values during DJF. The IVT variance over the full record exhibits a zonal band of enhanced variance in central North Pacific with a domain maximum at approximately 32°N, 180° that extends toward the northwestern United States (Fig. 5a). The high variance primarily results from the passage of midlatitude cyclones (see, e.g., Newman et al. 2012) and their alternating regions of enhanced (reduced) moisture transport on the eastern (western) side of cold fronts. Figures 5b–d show the 6-h IVT variance in each ENSO category divided by the total variance (Fig. 5a), where the significance of the change in the ENSO–total variance ratio is evaluated using an F test and only significant values are shaded. The

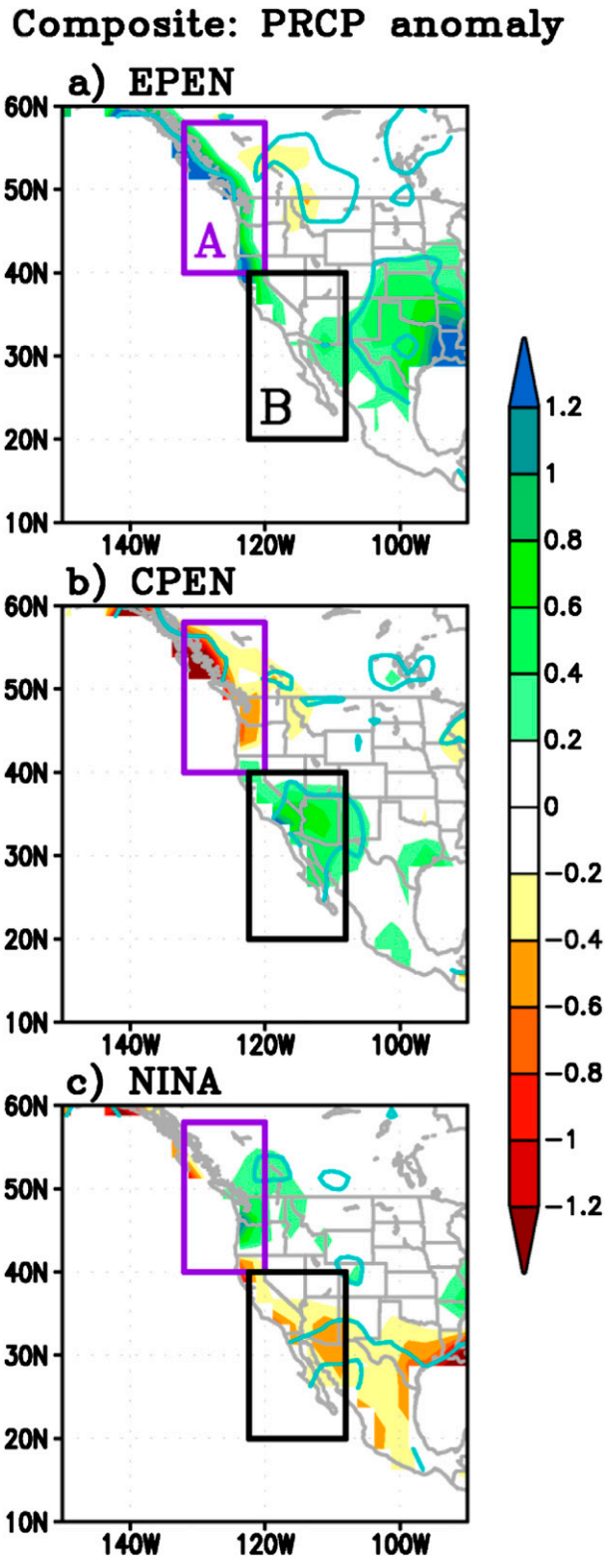

FIG. 3. Composite of seasonal mean (DJF) precipitation anomaly (mm day^{-1}) averaged only over the land area within the purple (region A) and black (region B) boxes for (a) EPEN, (b) CPEN, and (c) NINA. Aqua contours show statistical significance at the 90% level.

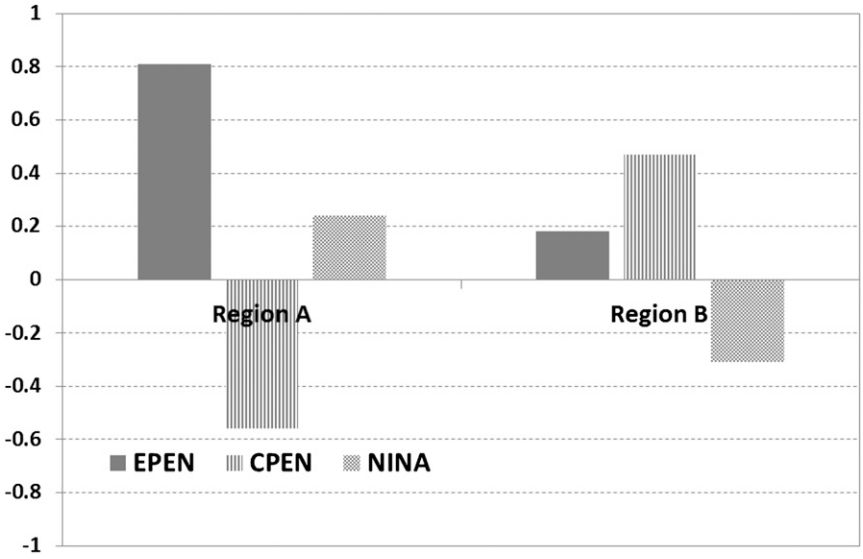

FIG. 4. Seasonal mean (DJF) precipitation anomaly (mm day^{-1}) averaged over regions A and B for EPEN (solid bar), CPEN (vertical stripe), and NINA (stippled bar).

IVT variability differs between the three ENSO categories. Relative to the total variance, the variance during EPEN (Fig. 5b) is greater over central Mexico (green/blue shading) and smaller over the subtropics and the western half of the United States. For CPEN (Fig. 5c), the variability is stronger over most of Mexico and the adjacent Pacific Ocean. The CPEN IVT variance is reduced over much of the North Pacific west of about 120°W with the exception of a narrow band that extends from approximately 25°N, 180° to the Washington coast (~47°N, 124°W). During NINA winters the variance is enhanced around 40°N over the central North Pacific Ocean and reduced across the all longitudes from approximately 20° to 30°N (Fig. 5d). The variability is also slightly greater (weaker) over portions of the southwestern (northwestern) United States.

We analyze the leading patterns of 6-h IVT variability and associated 500-hPa height anomalies based on empirical orthogonal function (EOF) analysis that is applied to 6-h IVT anomalies for the total period and for each of three ENSO categories. Given the wide range in IVT variability as a function of location, (e.g., it is much greater over the ocean than over land), we first normalize the anomalies by dividing them by the local standard deviation of the total 6-h IVT before computing the EOFs. We note that the eigenvectors (EOF patterns) are nearly identical between ENSO phases if the EOF analysis is performed using nonnormalized IVT anomalies (not shown). To emphasize the high IVT variability over western North America, we also computed EOFs using IVT values only over land. While this raises the percent variance explained by the leading EOFs and enhances the anomaly magnitude in specific geographic locations (Alexander et al. 2015), the patterns are not clearly distinguishable between the three ENSO phases (not shown).

The leading EOF for the full period and the three ENSO phases (Fig. 6) explains approximately 10% of the variance for EPEN and NINA, approximately 15% for CPEN, and approximately 12% for neutral years. The percentage variance explained is relatively low, since we use the 6-hourly anomalies with the biggest amplitude over the ocean, leading to patterns that are not tightly tied to specific geographic locations. While the state of ENSO influences the location and strength of winter storms and the large-scale moisture field, the overall IVT variability is still dominated by internal atmospheric processes associated with moving extratropical cyclones.

The second mode explains only a small amount of variance and is not distinguishable from the lower-order EOFs; therefore, we will only focus on the first mode. For the neutral years (Fig. 6a), the leading eigenvector is characterized by anomalies of one sign (positive for this phase of the EOF) that extends northeastward from the Hawaiian Islands to the southwestern United States, with a maximum over the far eastern Pacific. There is a much weaker anomaly of the opposite sign to the northwest. While the EOF by itself does not convey the sign and magnitude of the pattern associated with the EOF, the principal component (PC) does. The probability distribution of the leading PC (the time series of the phase and amplitude of the corresponding EOF), as indicated by a histogram of the first PC (PC1) values, is shown in Fig. 7. The distribution of PC1 for the neutral period is

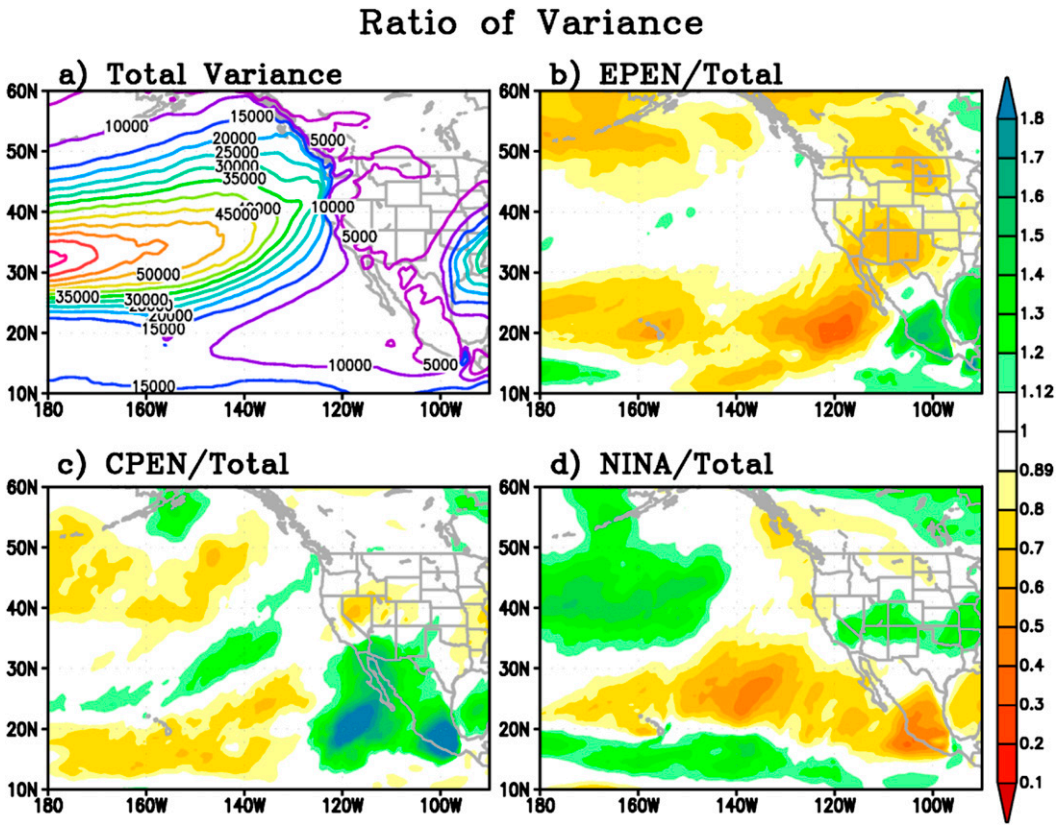

FIG. 5. (a) Total variance of the IVT computed by 6-h values during DJF from 1979 to 2010 and the ratio of variance for the 6-hourly IVT between (b) EPEN, (c) CPEN, and (d) NINA and the total variance. Shaded area indicates where the ratio of variance is statistically significant at the 99% level by an *F* test.

positively skewed (skewness is 0.69), indicating that very large positive IVT anomalies are more common than large negative values over the southwestern United States.

For EPEN, the first EOF (EOF1) pattern is similar to that in the neutral years, but the maximum is shifted to the north and west near 35°N, 135°W, and higher values extend into the northwestern rather than the southwestern United States (Fig. 6b). Anomalies of the opposite sign are found over the northwestern and southeastern corners of the domain. While the skewness of PC1 for EPEN is smaller than in the other ENSO phases, it is still positively skewed (skewness is 0.16), indicating that large positive IVT anomalies extending from the subtropical Pacific to the western United States are more common than large negative values in this region (Fig. 7). The EOF1 IVT pattern during CPEN has a pronounced dipole with a northern band that extends from the subtropics to the northwestern United States and a southern center located in the vicinity of Baja California (Fig. 6c). PC1 is positively skewed (Fig. 7; skewness is 0.26), indicating that large positive values are more common over Mexico and the southern United States than large negative values. For NINA, the EOF1 of IVT also exhibits a dipole with one center over California, Arizona, and New Mexico, and the opposite sign anomalies extending over the North Pacific Ocean from approximately 30°N, 170°W to 50°N, 140°W. The NINA PC1 values are also positively skewed (skewness is 0.21).

The IVT and 500-hPa height anomalies are examined using composite analysis of 6-hourly databased on the leading PC obtained from different ENSO phases. The composite averages are computed using the nonnormalized values at the times when PC1 is greater than positive two standard deviations for each of the ENSO phases. The IVT and Z500 anomaly composites are shown in Fig. 8. In neutral years (Fig. 8a), the composite IVT anomaly patterns are similar to the corresponding leading EOF, where the low pressure center is located just off the coast of California with a maximum around 38°N, 140°W. This trough exhibits a southwest–northeast tilt and the associated cyclonic circulation transports moisture from the subtropics to Baja California to nearly all of the U.S. West Coast.

Unlike the other periods, the moisture source appears to be primarily extratropical for EPEN (Fig. 8b), with a

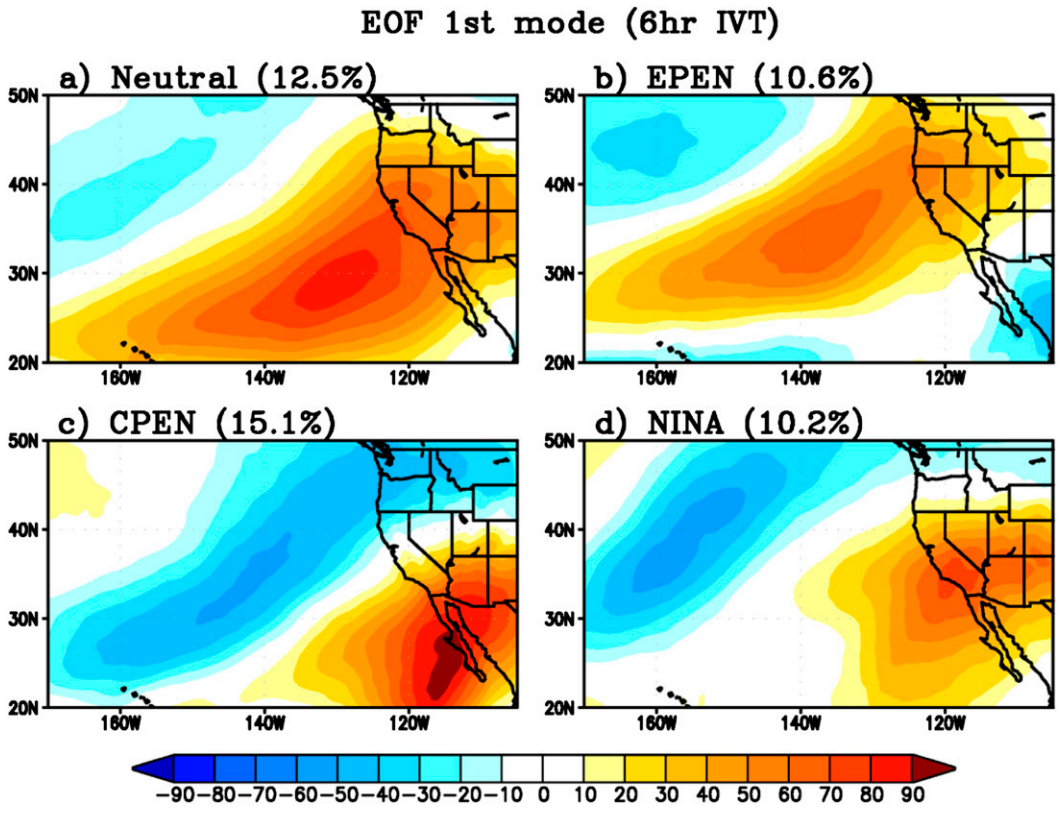

FIG. 6. Eigenvectors of the first EOF mode for 6-hourly IVT anomaly for (a) neutral years, (b) EPEN, (c) CPEN, and (d) NINA. Numbers indicate the percentage of variance of 6-hourly IVT anomalies in each ENSO phases. IVT anomalies are normalized by the total IVT daily standard deviation.

positive IVT anomaly extending from approximately 30°N, 160°W in the Pacific to the northwestern U.S. coast. The anomalous height pattern exhibits a very deep zonally elongated trough centered at approximately 41°N, 155°W, with a strong gradient along the eastern edge of the trough that parallels the northwestern U.S. coast, which is similar to the seasonal mean EPEN pattern (Fig. 1a). The strong low pressure anomaly induces strong moisture transport from the North Pacific toward the northwestern United States with large amount of transport into coastal Oregon but a modest amount on inland penetration of moisture (Fig. 8b). In EPEN winter, this circulation pattern occurs frequently and thus could result in enhanced seasonal precipitation in the northwestern United States (Fig. 3a).

For CPEN, a large positive IVT anomaly extends from the subtropical eastern Pacific Ocean across Baja California and Mexico and into the southwestern United States (Fig. 8c). The associated low pressure anomaly is shifted southeastward compared to EPEN and is located just off the California coast, where the cyclonic circulation induces a large amount of water vapor transport into the southwestern United States. The strong negative IVT anomaly over the northeastern Pacific Ocean is found along the strong gradient between the ridge centered at approximately 50°N, 140°W and a trough centered at approximately 30°N, 125°W, where the associated northeasterly

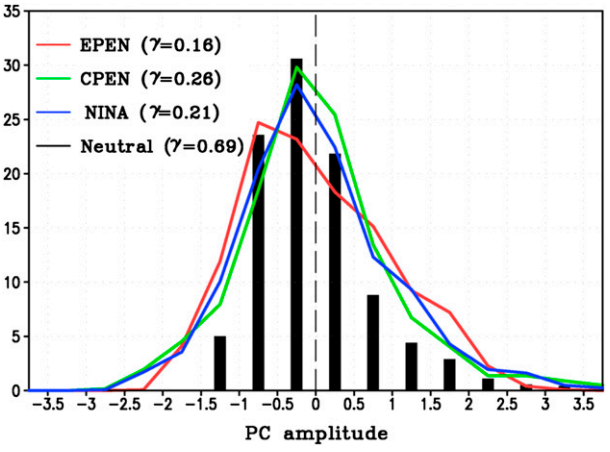

FIG. 7. Probability of EOF PC1 normalized value for neutral (black), EPEN (red), CPEN (green), and NINA (blue) phases. Numbers in parentheses indicate the skewness of the probability for each phase.

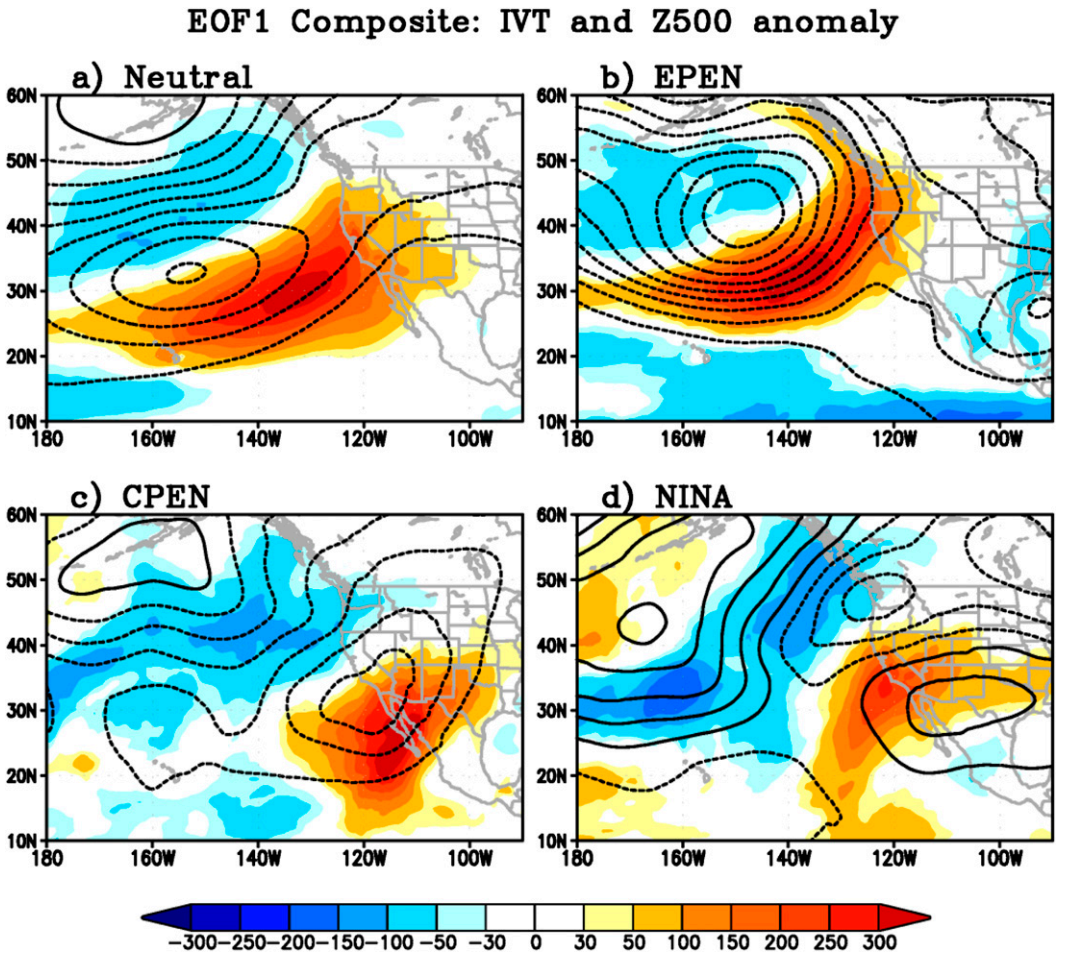

FIG. 8. EOF PC-based composites of 6-h 500-hPa height (m; contour interval is 30 m) and IVT ($kg\,m^{-1}\,s^{-1}$; shading) anomalies associated with the leading IVT EOF modes in each ENSO phase: (a) neutral, (b) EPEN, (c) CPEN, and (d) NINA.

flow transports colder/dryer air, some coming from North America, over the Pacific Ocean. Frequent occurrence of this pattern would result in heavy seasonal precipitation over the southwestern United States and a deficit in the northwestern United States and British Columbia (Fig. 3b).

For NINA, the dominant anomalous circulation is distinctly different from the patterns during both El Niño phases and the neutral years (Fig. 8d). For NINA, there are two high pressure anomalies, one over the southern United States and one over the North Pacific Ocean, with low pressure anomalies over the subtropics and northwestern United States. Moisture enters the southwestern United States via the anticyclonic circulation on the far western side of the ridge centered over Texas. The flow associated with the strong anticyclone over the North Pacific and cyclonic anomaly over the Pacific Northwest transports relatively cold/dry air from higher latitudes resulting in negative IVT anomalies from Canada to the central Pacific.

5. Summary and discussion

The change in the location and sign of SST anomalies in the tropical Pacific Ocean associated with different phases of ENSO alter the large-scale atmospheric state, and thus have different impacts on the climate over the Pacific–North American region. In this study, we investigate how the three phases of ENSO (i.e., eastern Pacific and central Pacific El Niños as well as La Niña; EPEN, CPEN, and NINA, respectively) modulate the atmospheric circulation and thereby change the water vapor transport into western North America.

In EPEN, large positive seasonal IVT anomalies extend northeastward from the subtropical Pacific into the northwestern United States following the anomalous

cyclonic flow around an anomalously deep Aleutian low. In CPEN, a southward shift of the cyclonic circulation over the North Pacific, which extends toward California, induces moisture transport into the southwestern United States. There is also a second IVT pathway into North America during CPEN; that is, moisture from the eastern tropical Pacific is transported across Mexico and into the southwestern United States. For NINA, the opposite circulation arises with an anticyclonic anomaly over the North Pacific and significant negative IVT anomalies at approximately 30°N on the southern side of this anticyclone.

The characteristics of the 6-h IVT anomalies during different ENSO phases have been explored by EOF and composite analyses. For EPEN, anomalous height pattern exhibits a very deep zonally elongated trough centered at approximately 40°N, 150°W, which induces strong moisture transport from the North Pacific to the northwestern U.S. coast but with a modest amount on inland penetration of moisture. For CPEN, the low pressure anomaly is shifted southeastward compared to EPEN and is located just off the California coast, where the cyclonic circulation induces a large amount of water vapor transport into the southwestern United States. For NINA, moisture enters the southwestern United States via anticyclonic circulation.

The water vapor transport associated with ARs is responsible for heavy snowfall and flooding events in western North America during winter. It is also the main source of water for the western United States (Ralph and Dettinger 2011), providing 25%–50% of California's water supply (Guan et al. 2013; Dettinger et al. 2011). A recent study by Alexander et al. (2015) found that during winter, moist air parcels from the Pacific take distinct pathways through gaps in the Cascades, Sierra Nevada, and peninsular mountains of Baja California, leading to extreme precipitation events in the U.S. Intermountain West. Our results indicate that CPEN events may enhance heavy precipitation in the southwestern states such as Arizona and New Mexico, but the overall influence of ENSO on the moisture transport into the U.S. Intermountain West and its predictability should be explored in greater detail.

In this study, we have used a high-resolution reanalysis that began in 1979, which includes satellite data. While this greatly improves the representation of ARs and IVT relative to coarse-resolution but longer reanalyses, it limits the composite analyses to just four cases for each ENSO phase. In addition, ENSO-related precipitation anomalies vary widely from episode to episode (e.g., Ropelewski and Halpert 1987). For example, the western United States was extremely dry during the 1976/77 El Niño but anomalously wet during the strong 1982/83 and 1997/98 El Niño events. Thus, the impact of variations in ENSO on water vapor transport and precipitation over the Pacific–North American region should be investigated further using longer datasets, where possible, and by model experiments.

Acknowledgments. The constructive and valuable comments of two reviewers are greatly appreciated. Kim was supported by the Korea Meteorological Administration Research and Development Program under Grant APCC 2013-3141. Alexander was supported by grants from the Bureau of Reclamation. We thank James D. Scott for providing the IVT data and Drs. Kathy Pegion (GMU) and Klaus Wolter (NOAA/ESRL) for their insightful suggestions.

REFERENCES

Adler, R. F., and Coauthors, 2003: The version 2 Global Precipitation Climatology Project (GPCP) monthly precipitation analysis (1979–present). *J. Hydrometeor.,* **4,** 1147–1167, doi:10.1175/1525-7541(2003)004<1147:TVGPCP>2.0.CO;2.

Alexander, M. A., J. D. Scott, D. Swales, M. Hughes, K. Mahoney, J. J. Barsugli, and C. Smith, 2015: Moisture pathways into the U.S. Intermountain West associated with heavy winter precipitation events. *J. Hydrometeor.,* doi:10.1175/JHM-D-14-0139.1, in press.

Ashok, K., S. K. Behera, S. A. Rao, H. Weng, and T. Yamagata, 2007: El Niño Modoki and its possible teleconnection. *J. Geophys. Res.,* **112,** C11007, doi:10.1029/2006JC003798.

Bao, J.-W., S. A. Michelson, P. J. Neiman, F. M. Ralph, and J. M. Wilczak, 2006: Interpretation of enhanced integrated water vapor bands associated with extratropical cyclones: Their formation and connection to tropical moisture. *Mon. Wea. Rev.,* **134,** 1063–1080, doi:10.1175/MWR3123.1.

Barsugli, J. J., and P. Sardeshmukh, 2002: Global atmospheric sensitivity to tropical SST anomalies throughout the Indo-Pacific basin. *J. Climate,* **15,** 3427–3442, doi:10.1175/1520-0442(2002)015<3427:GASTTS>2.0.CO;2.

Capotondi, A., and Coauthors, 2015: Understanding ENSO diversity. *Bull. Amer. Meteor. Soc.,* doi:10.1175/BAMS-D-13-00117.1, in press.

Dettinger, M. D., 2004: Fifty-two years of "pineapple-express" storms across the west coast of North America, PIER Energy-Related Environ. Res. Rep. CEC-500–2005-004, 15 pp.

——, F. M. Ralph, T. Das, P. J. Neiman, and D. R. Cayan, 2011: Atmospheric rivers, floods, and the water resources of California. *Water,* **3,** 445–478, doi:10.3390/w3020445.

Guan, B., D. E. Waliser, N. P. Molotch, E. J. Fetzer, and P. J. Neiman, 2012: Does the Madden–Julian oscillation influence wintertime atmospheric rivers and snowpack in the Sierra Nevada? *Mon. Wea. Rev.,* **140,** 325–342, doi:10.1175/MWR-D-11-00087.1.

——, N. P. Molotch, D. E. Waliser, E. J. Fetzer, and P. J. Neiman, 2013: The 2010/2011 snow season in California's Sierra Nevada: Role of atmospheric rivers and modes of large-scale variability. *Water Resour. Res.,* **49,** 6731–6743, doi:10.1002/wrcr.20537.

Jiang, T., and Y. Deng, 2011: Downstream modulation of North Pacific atmospheric river activity by East Asian cold surges. *Geophys. Res. Lett.,* **38,** L20807, doi:10.1029/2011GL049462.

——, K. J. Evans, Y. Deng, and X. Dong, 2014: Intermediate frequency atmospheric disturbances: A dynamical bridge connecting western U.S. extreme precipitation with East Asian cold surges. *J. Geophys. Res. Atmos.,* **119,** 3723–3735, doi:10.1002/2013JD021209.

Johnson, N. C., 2013: How many ENSO flavors can we distinguish? *J. Climate,* **26,** 4816–4827, doi:10.1175/JCLI-D-12-00649.1.

Kao, H.-Y., and J.-Y. Yu, 2009: Contrasting eastern-Pacific and central-Pacific types of ENSO. *J. Climate,* **22,** 615–632, doi:10.1175/2008JCLI2309.1.

Kug, J.-S., and Y.-G. Ham, 2011: Are there two types of La Niña events? *Geophys. Res. Lett.,* **38,** L16704, doi:10.1029/2011GL048237.

——, F.-F. Jin, and S.-I. An, 2009: Two types of El Niño events: Cold tongue El Niño and warm pool El Niño. *J. Climate,* **22,** 1499–1515, doi:10.1175/2008JCLI2624.1.

Lackmann, G. M., and J. R. Gyakum, 1999: Heavy cold-season precipitation in the northwestern United States: Synoptic climatology and an analysis of the flood of 17–18 January 1986. *Wea. Forecasting,* **14,** 687–700, doi:10.1175/1520-0434(1999)014<0687:HCSPIT>2.0.CO;2.

Larkin, N. K., and D. E. Harrison, 2002: ENSO warm (El Niño) and cold (La Niña) event life cycles: Ocean surface anomaly patterns, their symmetries, asymmetries, and implications. *J. Climate,* **15,** 1118–1140, doi:10.1175/1520-0442(2002)015<1118:EWENOA>2.0.CO;2.

Lee, T., and M. J. McPhaden, 2010: Increasing intensity of El Niño in the central-equatorial Pacific. *Geophys. Res. Lett.,* **37,** L14603, doi:10.1029/2010GL044007.

Madden, R. A., and P. R. Julian, 1972: Description of global-scale circulation cells in the tropics with a 40–50 day period. *J. Atmos. Sci.,* **29,** 1109–1123, doi:10.1175/1520-0469(1972)029<1109:DOGSCC>2.0.CO;2.

Mo, K., 2010: Interdecadal modulation of the impact of ENSO on precipitation and temperature over the United States. *J. Climate,* **23,** 3639–3656, doi:10.1175/2010JCLI3553.1.

Neiman, P. J., F. M. Ralph, G. A. Wick, J. D. Lundquist, and M. D. Dettinger, 2008: Meteorological characteristics and overland precipitation impacts of atmospheric rivers affecting the West Coast of North America based on eight years of SSM/I satellite observations. *J. Hydrometeor.,* **9,** 22–47, doi:10.1175/2007JHM855.1.

——, L. J. Schick, F. M. Ralph, M. Hughes, and G. A. Wick, 2011: Flooding in western Washington: The connection to atmospheric rivers. *J. Hydrometeor.,* **12,** 1337–1358, doi:10.1175/2011JHM1358.1.

Newell, R. E., N. E. Newell, Y. Zhu, and C. Scott, 1992: Tropospheric rivers? A pilot study. *Geophys. Res. Lett.,* **19,** 2401–2404, doi:10.1029/92GL02916.

Newman, M., M. A. Alexander, and J. D. Scott, 2011a: An empirical model of tropical ocean dynamics. *Climate Dyn.,* **37,** 1823–1841, doi:10.1007/s00382-011-1034-0.

——, S.-I. Shin, and M. A. Alexander, 2011b: Natural variation in ENSO flavors. *Geophys. Res. Lett.,* **38,** L14705, doi:10.1029/2011GL047658.

——, G. N. Kiladis, K. M. Weickmann, F. M. Ralph, and P. D. Sardeshmukh, 2012: Relative contributions of synoptic and low-frequency eddies to time-mean atmospheric moisture transport, including the role of atmospheric rivers. *J. Climate,* **25,** 7341–7361, doi:10.1175/JCLI-D-11-00665.1.

Ralph, F. M., and M. D. Dettinger, 2011: Storms, floods and the science of atmospheric rivers. *Eos, Trans. Amer. Geophys. Union,* **92,** 265–266, doi:10.1029/2011EO320001.

——, P. J. Neiman, G. A. Wick, S. I. Gutman, M. D. Dettinger, D. R. Cayan, and A. B. White, 2006: Flooding on California's Russian River: Role of atmospheric rivers. *Geophys. Res. Lett.,* **33,** L13801, doi:10.1029/2006GL026689.

Reynolds, R. W., N. A. Rayner, T. M. Smith, D. C. Stokes, and W. Wang, 2002: An improved in situ and satellite SST analysis for climate. *J. Climate,* **15,** 1609–1625, doi:10.1175/1520-0442(2002)015<1609:AIISAS>2.0.CO;2.

Ropelewski, C. F., and M. S. Halpert, 1987: Global and regional scale precipitation patterns associated with the El Niño/Southern Oscillation. *Mon. Wea. Rev.,* **115,** 1606–1626, doi:10.1175/1520-0493(1987)115<1606:GARSPP>2.0.CO;2.

Rutz, J. J., W. J. Steenburgh, and F. M. Ralph, 2014: Climatological characteristics of atmospheric rivers and their inland penetration over the western United States. *Mon. Wea. Rev.,* **142,** 905–921, doi:10.1175/MWR-D-13-00168.1.

Saha, S., and Coauthors, 2010: The NCEP Climate Forecast System Reanalysis. *Bull. Amer. Meteor. Soc.,* **91,** 1015–1057, doi:10.1175/2010BAMS3001.1.

van Oldenborgh, G. J., and G. Burgers, 2005: Searching for decadal variations in ENSO precipitation teleconnections. *Geophys. Res. Lett.,* **32,** L15701, doi:10.1029/2005GL023110.

Waliser, D. E., B. Guan, J.-L. Li, and J. Kim, 2012: Addendum to "Simulating cold season snowpack: Impacts of snow albedo and multi-layer snow physics": Waliser, D., J. Kim, Y. Xue, Y. Chao, A. Eldering, R. Fovell, A. Hall, Q. Li, K. N. Liou, J. McWilliams, S. Kapnick, R. Vasic, F. De Sale, and Y. Yu (2011), *Climatic Change,* 109 (Suppl 1): S95–S117, doi:10.1007/s10584-011-0312-5. *Climate Change,* **114,** 399–400, doi:10.1007/s10584-012-0531-4.

Warner, M. D., C. F. Mass, and E. P. Salathé, 2012: Wintertime extreme precipitation events along the Pacific Northwest coast: Climatology and synoptic evolution. *Mon. Wea. Rev.,* **140,** 2021–2043, doi:10.1175/MWR-D-11-00197.1.

Yeh, S.-W., J. S. Kug, B. Dewitte, M.-H. Kwon, B. Kirtman, and F.-F. Jin, 2009: Recent changes in El Niño and its projection under global warming. *Nature,* **461,** 511–515, doi:10.1038/nature08316.

Yu, J.-Y., and Y. Zou, 2013: The enhanced drying effect of Central-Pacific El Niño on US winter. *Environ. Res. Lett.,* **8,** 014019, doi:10.1088/1748-9326/8/1/014019.

——, ——, S. T. Kim, and T. Lee, 2012: The changing impact of El Niño on US winter temperatures. *Geophys. Res. Lett.,* **39,** L15702, doi:10.1029/2012GL052483.

Zhu, Y., and R. Newell, 1998: A proposed algorithm for moisture fluxes from atmospheric rivers. *Mon. Wea. Rev.,* **126,** 725–735, doi:10.1175/1520-0493(1998)126<0725:APAFMF>2.0.CO;2.